Eur. Phys. J. C 12, 53–68 (2000)
Digital Object Identifier (DOI) 10.1007/s100529900245

THE EUROPEAN PHYSICAL JOURNAL C

Angular and current-target correlations in deep inelastic scattering at HERA

The ZEUS Collaboration

J. Breitweg, S. Chekanov, M. Derrick, D. Krakauer, S. Magill, B. Musgrave, A. Pellegrino, J. Repond, R. Stanek, R. Yoshida
Argonne National Laboratory, Argonne, IL, USA [p]

M.C.K. Mattingly
Andrews University, Berrien Springs, MI, USA

G. Abbiendi, F. Anselmo, P. Antonioli, G. Bari, M. Basile, L. Bellagamba, D. Boscherini[1], A. Bruni, G. Bruni, G. Cara Romeo, G. Castellini[2], L. Cifarelli[3], F. Cindolo, A. Contin, N. Coppola, M. Corradi, S. De Pasquale, P. Giusti, G. Iacobucci[4], G. Laurenti, G. Levi, A. Margotti, T. Massam, R. Nania, F. Palmonari, A. Pesci, A. Polini, G. Sartorelli, Y. Zamora Garcia[5], A. Zichichi
University and INFN Bologna, Bologna, Italy [f]

C. Amelung, A. Bornheim, I. Brock, K. Coböken, J. Crittenden, R. Deffner, M. Eckert[6], H. Hartmann, K. Heinloth, L. Heinz[7], E. Hilger, H.-P. Jakob, A. Kappes, U.F. Katz, R. Kerger, E. Paul, M. Pfeiffer[8], J. Rautenberg, H. Schnurbusch, A. Stifutkin, J. Tandler, A. Weber, H. Wieber
Physikalisches Institut der Universität Bonn, Bonn, Germany [c]

D.S. Bailey, O. Barret, W.N. Cottingham, B. Foster[9], G.P. Heath, H.F. Heath, J.D. McFall, D. Piccioni, J. Scott, R.J. Tapper
H.H. Wills Physics Laboratory, University of Bristol, Bristol, UK [o]

M. Capua, A. Mastroberardino, M. Schioppa, G. Susinno
Calabria University, Physics Departmentand INFN, Cosenza, Italy [f]

H.Y. Jeoung, J.Y. Kim, J.H. Lee, I.T. Lim, K.J. Ma, M.Y. Pac[10]
Chonnam National University, Kwangju, Korea [h]

A. Caldwell, N. Cartiglia, Z. Jing, W. Liu, B. Mellado, J.A. Parsons, S. Ritz[11], R. Sacchi, S. Sampson, F. Sciulli, Q. Zhu[12]
Columbia University, Nevis Labs., Irvington on Hudson, N.Y., USA [q]

P. Borzemski, J. Chwastowski, A. Eskreys, J. Figiel, K. Klimek, K. Olkiewicz, M.B. Przybycień, L. Zawiejski
Inst. of Nuclear Physics, Cracow, Poland [j]

L. Adamczyk[13], B. Bednarek, K. Jeleń, D. Kisielewska, A.M. Kowal, T. Kowalski, M. Przybycień, E. Rulikowska-Zarębska, L. Suszycki, J. Zając
Faculty of Physics and Nuclear Techniques, Academy of Mining and Metallurgy, Cracow, Poland [j]

Z. Duliński, A. Kotański
Jagellonian University, Department of Physics, Cracow, Poland [k]

L.A.T. Bauerdick, U. Behrens, J.K. Bienlein, C. Burgard, K. Desler, G. Drews, A. Fox-Murphy, U. Fricke, F. Goebel, P. Göttlicher, R. Graciani, T. Haas, W. Hain, G.F. Hartner, D. Hasell[14], K. Hebbel, K.F. Johnson[15], M. Kasemann[16], W. Koch, U. Kötz, H. Kowalski, L. Lindemann, B. Löhr, M. Martínez, J. Milewski[17], M. Milite,

T. Monteiro[18], M. Moritz, D. Notz, F. Pelucchi, K. Piotrzkowski, M. Rohde, P.R.B. Saull, A.A. Savin, U. Schneekloth, O. Schwarzer[19], F. Selonke, M. Sievers, S. Stonjek, E. Tassi, G. Wolf, U. Wollmer, C. Youngman, W. Zeuner
Deutsches Elektronen-Synchrotron DESY, Hamburg, Germany

B.D. Burow[20], C. Coldewey, H.J. Grabosch, A. Lopez-Duran Viani, A. Meyer, K. Mönig, S. Schlenstedt, P.B. Straub
DESY Zeuthen, Zeuthen, Germany

G. Barbagli, E. Gallo, P. Pelfer
University and INFN, Florence, Italy [f]

G. Maccarrone, L. Votano
INFN, Laboratori Nazionali di Frascati, Frascati, Italy [f]

A. Bamberger, S. Eisenhardt[21], P. Markun, H. Raach, S. Wölfle
Fakultät für Physik der Universität Freiburg i.Br., Freiburg i.Br., Germany [c]

N.H. Brook[22], P.J. Bussey, A.T. Doyle, S.W. Lee, N. Macdonald, G.J. McCance, D.H. Saxon, L.E. Sinclair, I.O. Skillicorn, E. Strickland, R. Waugh
Department of Physics and Astronomy, University of Glasgow, Glasgow, UK [o]

I. Bohnet, N. Gendner, U. Holm, A. Meyer-Larsen, H. Salehi, K. Wick
Hamburg University, I. Institute of Exp. Physics, Hamburg, Germany [c]

A. Garfagnini, I. Gialas[23], L.K. Gladilin[24], D. Kçira[25], R. Klanner, E. Lohrmann, G. Poelz, F. Zetsche
Hamburg University, II. Institute of Exp. Physics, Hamburg, Germany [c]

T.C. Bacon, J.E. Cole, G. Howell, L. Lamberti[26], K.R. Long, D.B. Miller, A. Prinias[27], J.K. Sedgbeer, D. Sideris, A.D. Tapper, R. Walker
Imperial College London, High Energy Nuclear Physics Group, London, UK [o]

U. Mallik, S.M. Wang
University of Iowa, Physics and Astronomy Department, Iowa City, USA [p]

P. Cloth, D. Filges
Forschungszentrum Jülich, Institut für Kernphysik, Jülich, Germany

T. Ishii, M. Kuze, I. Suzuki[28], K. Tokushuku[29], S. Yamada, K. Yamauchi, Y. Yamazaki
Institute of Particle and Nuclear Studies, KEK, Tsukuba, Japan [g]

S.H. Ahn, S.H. An, S.J. Hong, S.B. Lee, S.W. Nam[30], S.K. Park
Korea University, Seoul, Korea [h]

H. Lim, I.H. Park, D. Son
Kyungpook National University, Taegu, Korea [h]

F. Barreiro, J.P. Fernández, G. García, C. Glasman[31], J.M. Hernández[32], L. Labarga, J. del Peso, J. Puga, I. Redondo[33], J. Terrón
Univer. Autónoma Madrid, Depto de Física Teórica, Madrid, Spain [n]

F. Corriveau, D.S. Hanna, J. Hartmann[34], W.N. Murray[6], A. Ochs, S. Padhi, M. Riveline, D.G. Stairs, M. St-Laurent, M. Wing
McGill University, Department of Physics, Montréal, Québec, Canada [a], [b]

T. Tsurugai
Meiji Gakuin University, Faculty of General Education, Yokohama, Japan

V. Bashkirov[35], B.A. Dolgoshein
Moscow Engineering Physics Institute, Moscow, Russia [l]

G.L. Bashindzhagyan, P.F. Ermolov, Yu.A. Golubkov, L.A. Khein, N.A. Korotkova, I.A. Korzhavina, V.A. Kuzmin, O.Yu. Lukina, A.S. Proskuryakov, L.M. Shcheglova[36], A.N. Solomin[36], S.A. Zotkin
Moscow State University, Institute of Nuclear Physics, Moscow, Russia [m]

C. Bokel, M. Botje, N. Brümmer, J. Engelen, E. Koffeman, P. Kooijman, A. van Sighem, H. Tiecke, N. Tuning, J.J. Velthuis, W. Verkerke, J. Vossebeld, L. Wiggers, E. de Wolf
NIKHEF and University of Amsterdam, Amsterdam, The Netherlands [i]

D. Acosta[37], B. Bylsma, L.S. Durkin, J. Gilmore, C.M. Ginsburg, C.L. Kim, T.Y. Ling, P. Nylander
Ohio State University, Physics Department, Columbus, Ohio, USA [p]

H.E. Blaikley, S. Boogert, R.J. Cashmore[18], A.M. Cooper-Sarkar, R.C.E. Devenish, J.K. Edmonds, J. Große-Knetter[38], N. Harnew, T. Matsushita, V.A. Noyes[39], A. Quadt[18], O. Ruske, M.R. Sutton, R. Walczak, D.S. Waters
Department of Physics, University of Oxford, Oxford, UK [o]

A. Bertolin, R. Brugnera, R. Carlin, F. Dal Corso, S. Dondana, U. Dosselli, S. Dusini, S. Limentani, M. Morandin, M. Posocco, L. Stanco, R. Stroili, C. Voci
Dipartimento di Fisica dell' Università and INFN, Padova, Italy [f]

L. Iannotti[40], B.Y. Oh, J.R. Okrasiński, W.S. Toothacker, J.J. Whitmore
Pennsylvania State University, Department of Physics, University Park, PA, USA [q]

Y. Iga
Polytechnic University, Sagamihara, Japan [g]

G. D'Agostini, G. Marini, A. Nigro, M. Raso
Dipartimento di Fisica, University 'La Sapienza' and INFN, Rome, Italy [f]

C. Cormack, J.C. Hart, N.A. McCubbin, T.P. Shah
Rutherford Appleton Laboratory, Chilton, Didcot, Oxon, UK [o]

D. Epperson, C. Heusch, H.F.-W. Sadrozinski, A. Seiden, R. Wichmann, D.C. Williams
University of California, Santa Cruz, CA, USA [p]

N. Pavel
Fachbereich Physik der Universität-Gesamthochschule Siegen, Germany [c]

H. Abramowicz[41], S. Dagan[42], S. Kananov[42], A. Kreisel, A. Levy[42], A. Schechter
Raymond and Beverly Sackler Faculty of Exact Sciences, School of Physics, Tel-Aviv University, Tel-Aviv, Israel [e]

T. Abe, T. Fusayasu, M. Inuzuka, K. Nagano, K. Umemori, T. Yamashita
Department of Physics, University of Tokyo, Tokyo, Japan [g]

R. Hamatsu, T. Hirose, K. Homma[43], S. Kitamura[44], T. Nishimura
Tokyo Metropolitan University, Department of Physics, Tokyo, Japan [g]

M. Arneodo[45], R. Cirio, M. Costa, M.I. Ferrero, S. Maselli, V. Monaco, C. Peroni, M.C. Petrucci, M. Ruspa, A. Solano, A. Staiano
Università di Torino, Dipartimento di Fisica Sperimentale and INFN, Torino, Italy [f]

M. Dardo
II Faculty of Sciences, Torino University and INFN - Alessandria, Italy [f]

D.C. Bailey, C.-P. Fagerstroem, R. Galea, T. Koop, G.M. Levman, J.F. Martin, R.S. Orr, S. Polenz, A. Sabetfakhri, D. Simmons
University of Toronto, Department of Physics, Toronto, Ont., Canada [a]

J.M. Butterworth, C.D. Catterall, M.E. Hayes, E.A. Heaphy, T.W. Jones, J.B. Lane
University College London, Physics and Astronomy Department, London, UK [o]

J. Ciborowski, G. Grzelak[46], R.J. Nowak, J.M. Pawlak, R. Pawlak, B. Smalska, T. Tymieniecka, A.K. Wróblewski, J.A. Zakrzewski, A.F. Żarnecki
Warsaw University, Institute of Experimental Physics, Warsaw, Poland [j]

M. Adamus, T. Gadaj
Institute for Nuclear Studies, Warsaw, Poland [j]

O. Deppe, Y. Eisenberg[42], D. Hochman, U. Karshon[42]
Weizmann Institute, Department of Particle Physics, Rehovot, Israel [d]

W.F. Badgett, D. Chapin, R. Cross, C. Foudas, S. Mattingly, D.D. Reeder, W.H. Smith, A. Vaiciulis[47], T. Wildschek, M. Wodarczyk
University of Wisconsin, Department of Physics, Madison, WI, USA [p]

A. Deshpande, S. Dhawan, V.W. Hughes
Yale University, Department of Physics, New Haven, CT, USA [p]

S. Bhadra, W.R. Frisken, R. Hall-Wilton, M. Khakzad, S. Menary, W.B. Schmidke
York University, Department of Physics, Toronto, Ont., Canada [a]

Received: 18 May 1999 / Published online: 3 November 1999

Abstract. Correlations between charged particles in deep inelastic e^+p scattering have been studied in the Breit frame with the ZEUS detector at HERA using an integrated luminosity of $6.4\,\mathrm{pb}^{-1}$. Short-range correlations are analysed in terms of the angular separation between current-region particles within a cone centred around the virtual photon axis. Long-range correlations between the current and target regions have also been measured. The data support predictions for the scaling behaviour of the angular correlations at high Q^2 and for anti-correlations between the current and target regions over a large range in Q^2 and in the Bjorken scaling variable x. Analytic QCD calculations and Monte Carlo models correctly describe the trends of the data at high Q^2, but show quantitative discrepancies. The data show differences between the correlations in deep inelastic scattering and e^+e^- annihilation.

[1] now visiting scientist at DESY
[2] also at IROE Florence, Italy
[3] now at University of Salerno and INFN Napoli, Italy
[4] also at DESY
[5] supported by Worldlab, Lausanne, Switzerland
[6] now a self-employed consultant
[7] now at Spectral Design GmbH, Bremen
[8] now at EDS Electronic Data Systems GmbH, Troisdorf, Germany
[9] also at University of Hamburg, Alexander von Humboldt Research Award
[10] now at Dongshin University, Naju, Korea
[11] now at NASA Goddard Space Flight Center, Greenbelt, MD 20771, USA
[12] now at Greenway Trading LLC
[13] supported by the Polish State Committee for Scientific Research, grant No. 2P03B14912
[14] now at Massachusetts Institute of Technology, Cambridge, MA, USA
[15] visitor from Florida State University
[16] now at Fermilab, Batavia, IL, USA
[17] now at ATM, Warsaw, Poland
[18] now at CERN
[19] now at ESG, Munich
[20] now an independent researcher in computing
[21] now at University of Edinburgh, Edinburgh, UK
[22] PPARC Advanced fellow
[23] visitor of University of Crete, Greece, partially supported by DAAD, Bonn - Kz. A/98/16764
[24] on leave from MSU, supported by the GIF, contract I-0444-176.07/95
[25] supported by DAAD, Bonn - Kz. A/98/12712
[26] supported by an EC fellowship
[27] PPARC Post-doctoral fellow
[28] now at Osaka University, Osaka, Japan
[29] also at University of Tokyo
[30] now at Wayne State University, Detroit
[31] supported by an EC fellowship number ERBFMBICT 972523
[32] now at HERA-B/DESY supported by an EC fellowship No.ERBFMBICT 982981
[33] supported by the Comunidad Autonoma de Madrid
[34] now at debis Systemhaus, Bonn, Germany
[35] now at Loma Linda University, Loma Linda, CA, USA
[36] partially supported by the Foundation for German-Russian Collaboration DFG-RFBR
(grant no. 436 RUS 113/248/3 and no. 436 RUS 113/248/2)
[37] now at University of Florida, Gainesville, FL, USA

1 Introduction

This paper reports a study of both short-range and long-range correlations in neutral-current deep inelastic e^+p scattering events measured at a centre-of-mass energy of $\sqrt{s} = 300\,\text{GeV}$ with the ZEUS detector at HERA.

In deep inelastic scattering (DIS) at HERA energies, final-state charged particles have been studied in terms of fragmentation functions [1–4], transverse momentum spectra [5, 6] and particle correlations [7–9]. The short-range correlations between final-state particles at small phase-space separations are sensitive to the structure of many-particle inclusive densities [10]. The study of long-range correlations can aid the understanding of the interdependence between distant phase-space regions; these measurements complement and extend the studies of the global multiplicity distributions that have already been reported in DIS [1, 3, 11] at HERA energies.

Two-particle angular correlations have recently been studied in e^+e^- collisions by the DELPHI Collaboration [12] at LEP and many-particle correlations have also been measured by the L3 [13] and OPAL Collaborations [14]. Such studies provide more detailed insight into the QCD models (see reviews [15,16]) based on the hypothesis of Local Parton-Hadron Duality, which states that the single-particle distributions of hadrons are proportional to the corresponding parton spectra [17]. The analytic predictions, derived in the Double Log Approximation (DLA) [18–20], have shown discrepancies with the observed angular correlations as well as with the fluctuation measurements [12, 13]. The DLA calculations take into account the contributions from the infrared and collinear singularities of the gluon emissions and the angular ordering (colour coherence), but neglect energy-momentum conservation in gluon splittings and $q\bar{q}$ production as well as finite-energy effects in the QCD parton cascade. However, Monte Carlo (MC) models which take these effects into account and which, in addition, contain hadronisation followed by resonance decays, also show discrepancies with the data [13, 14].

DIS provides a unique possibility to confront both the analytic results and MC models with data at various energy scales. The main motivation for such studies is to investigate the applicability of the perturbative analytic calculations to DIS data at HERA energies. The two-particle angular correlations in the current region of the Breit frame are also compared with the correlations in a single hemisphere of e^+e^- annihilation in order to study a possible universality of two-particle spectra in these processes. Recent comparisons of single-particle spectra have shown considerable similarity between DIS at high Q^2 and e^+e^- annihilation [1–4, 11].

Correlations between distant phase-space regions provide important information on multi-hadron production that cannot be studied by measuring observables separately in each phase-space region. In DIS, a measurement of the correlations between the hemisphere populated by hadrons originating from the struck quark and that containing predominantly particles from the proton remnant can be made in a way analogous to "forward-backward" correlations. Such long-range correlations in rapidity have been studied for many years [9, 21–28]. Results for e^+e^- and μ^+p processes indicated that such correlations are

[38] supported by the Feodor Lynen Program of the Alexander von Humboldt foundation
[39] now with Physics World, Dirac House, Bristol, UK
[40] partly supported by Tel Aviv University
[41] an Alexander von Humboldt Fellow at University of Hamburg
[42] supported by a MINERVA Fellowship
[43] now at ICEPP, University of Tokyo, Tokyo, Japan
[44] present address: Tokyo Metropolitan University of Health Sciences, Tokyo 116-8551, Japan
[45] now also at Università del Piemonte Orientale, I-28100 Novara, Italy, and Alexander von Humboldt fellow at the University of Hamburg
[46] supported by the Polish State Committee for Scientific Research, grant No. 2P03B09308
[47] now at University of Rochester, Rochester, NY, USA
[a] supported by the Natural Sciences and Engineering Research Council of Canada (NSERC)
[b] supported by the FCAR of Québec, Canada
[c] supported by the German Federal Ministry for Education and Science, Research and Technology (BMBF), under contract numbers 057BN19P, 057FR19P, 057HH19P, 057HH29P, 057SI75I
[d] supported by the MINERVA Gesellschaft für Forschung GmbH, the German Israeli Foundation, and by the Israel Ministry of Science
[e] supported by the German-Israeli Foundation, the Israel Science Foundation, the U.S.-Israel Binational Science Foundation, and by the Israel Ministry of Science
[f] supported by the Italian National Institute for Nuclear Physics (INFN)
[g] supported by the Japanese Ministry of Education, Science and Culture (the Monbusho) and its grants for Scientific Research
[h] supported by the Korean Ministry of Education and Korea Science and Engineering Foundation
[i] supported by the Netherlands Foundation for Research on Matter (FOM)
[j] supported by the Polish State Committee for Scientific Research, grant No. 115/E-343/SPUB/P03/154/98, 2P03B03216, 2P03B04616, 2P03B10412, 2P03B05315, and by the German Federal Ministry of Education and Science, Research and Technology (BMBF)
[k] supported by the Polish State Committee for Scientific Research (grant No. 2P03B08614 and 2P03B06116)
[l] partially supported by the German Federal Ministry for Education and Science, Research and Technology (BMBF)
[m] supported by the Fund for Fundamental Research of Russian Ministry for Science and Education and by the German Federal Ministry for Education and Science, Research and Technology (BMBF)
[n] supported by the Spanish Ministry of Education and Science through funds provided by CICYT
[o] supported by the Particle Physics and Astronomy Research Council
[p] supported by the US Department of Energy
[q] supported by the US National Science Foundation

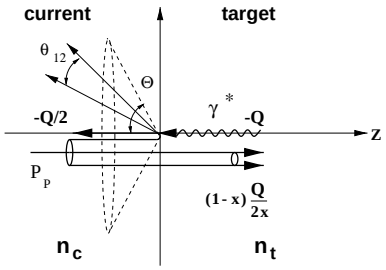

Fig. 1. A schematic representation of the measurement of correlations in the Breit frame. The angular correlations in the current region are measured between any two charged particles separated by θ_{12}. Long-range correlations in the full phase space are measured between current (n_c) and target (n_t) multiplicities

small at low energies [21, 22]. At LEP1 energies, positive long-range correlations were observed, mainly due to heavy quark pair production [23–25]. For νp and $\overline{\nu}p$ processes, the correlations are small and negative [26]. For pp, $p\overline{p}$ [27] and $\pi^{\pm}p$, $K^{+}p$ [28] collisions, the correlations are positive and increase with $\sqrt{s}$. Recently, the H1 Collaboration has shown that the forward-backward correlations measured in the γ^*-pomeron centre-of-mass system of diffractive e^+p collisions are positive [9]. In contrast, in the Breit frame in DIS, negative long-range correlations due to the kinematics of first-order QCD effects have been predicted [29].

2 Definitions and analytic QCD results

2.1 DIS kinematics in the Breit frame

The event kinematics of DIS processes are determined by the negative squared 4-momentum transfer at the lepton vertex, $Q^2 = -q^2 = -(k - k')^2$ (k and k' denote the 4-momenta of the initial and final-state positron, respectively), and the Bjorken scaling variable $x = Q^2/(2P_{\rm p} \cdot q)$, where $P_{\rm p}$ is the 4-momentum of the proton. The fractional energy transfer to the proton in its rest frame, y, is related to these two variables by $y \simeq Q^2/xs$, where $\sqrt{s}$ is the positron-proton centre-of-mass energy.

The correlations are studied in the Breit frame [30], which provides a natural system to separate the radiation from the outgoing struck quark from that associated with the rest of the hadronic final state. In this frame, the exchanged virtual boson is completely space-like and has a momentum $q = (q_0, q_X, q_Y, q_Z) = (0, 0, 0, -Q)$ as shown in Fig. 1. For the Quark-Parton Model (QPM), the incident quark carries Z-momentum $p_Z^{\rm Breit} = Q/2$ in the positive Z-direction and the outgoing struck quark carries $p_Z^{\rm Breit} = -Q/2$ in the negative Z-direction. The phase space of the event can be divided into two regions. All particles with negative $p_Z^{\rm Breit}$ form the current region. These particles are produced by the fragmentation of the struck quark, so that the current region is analogous to a single hemisphere of e^+e^- annihilation. Particles with positive $p_Z^{\rm Breit}$ are assigned to the target region associated with the incoming proton. The longitudinal phase space in $p_Z^{\rm Breit}$ available for the target-region particles extends to $p_Z^{\rm Breit} = (1-x)Q/2x$. This means that the current and target regions are highly asymmetric at small x. Thus the Breit frame differs from the hadronic centre-of-mass (γ^*p) frame and the centre-of-mass frame of e^+e^- annihilation.

This simple picture of DIS in the Breit frame is changed when leading-order QCD processes, Boson-Gluon Fusion (BGF) and QCD-Compton (QCDC) scattering, are considered. In such processes, the collision in the Breit frame is no longer collinear, although the current and target regions are still well-defined operationally [31].

2.2 Two-particle correlations

The correlations between charged particles in the current region are studied using the angle between any two particles (see Fig. 1). For each pair of particles inside a cone of half-angle Θ centred around the Breit frame axis, the relative angle θ_{12} is determined. For a given QCD scale, Λ, this angle is transformed into the variable

$$\varepsilon = \frac{\ln(\Theta/\theta_{12})}{\ln(P \sin\Theta/\Lambda)}, \qquad (1)$$

For DIS in the Breit frame, $P = Q/2$ is chosen, corresponding to the outgoing quark momentum in the QPM. Note that Λ is an effective scale parameter which is not related to $\Lambda_{\overline{\rm MS}}$ [12]. The two-particle inclusive density

$$\rho(\varepsilon) = \frac{1}{N_{\rm ev}} \frac{dn_{\rm pair}}{d\varepsilon} \qquad (2)$$

is determined, where $N_{\rm ev}$ is the number of events and $(dn_{\rm pair}/d\varepsilon)\delta\varepsilon$ is the number of particle pairs in the interval ε to $\varepsilon + \delta\varepsilon$. The definition (1) is used since the DLA predictions can be naturally expressed in this scaling variable [18,20] and the logarithmic dependence of (1) expands small values of θ_{12}. Note that our definition of ε is different from the scaling variable with the denominator $\ln(P\Theta/\Lambda)$ used previously [12,13]: for large Θ, the definition (1) is better suited to compare the DLA predictions with the data [32].

In this paper we measure the relative angular distribution $\hat{r}(\varepsilon)$ and the correlation function $r(\varepsilon)$:

$$\hat{r}(\varepsilon) = \frac{\rho(\varepsilon)}{\langle n(\Theta)\rangle^2}, \qquad r(\varepsilon) = \frac{\rho(\varepsilon)}{\rho_{\rm mix}(\varepsilon)}. \qquad (3)$$

The variable $\hat{r}(\varepsilon)$ is $\rho(\varepsilon)$ normalised using the average charged multiplicity $\langle n(\Theta)\rangle$ in the cone. Even for uncorrelated particle production, $\hat{r}(\varepsilon)$ depends on ε in a manner which is determined by the single-particle spectra. This dependence is reduced in $r(\varepsilon)$, which is normalised instead by $\rho_{\rm mix}(\varepsilon)$, calculated using particles from *different* events. Thus $\rho_{\rm mix}(\varepsilon)$ does not contain any of the dynamical correlation present among particles from the same event, but is

sensitive to effects determined by the single-particle spectra. To obtain $\rho_{\rm mix}(\varepsilon)$, each of the original tracks in an event is replaced by a track selected at random from all the other events. This is performed after the transformation of the real events to the Breit frame. These "fake" events are then used to calculate $\rho_{\rm mix}(\varepsilon)$ in exactly the same way as $\rho(\varepsilon)$ is calculated from the real events. It should be noted that each fake event has, by construction, the same multiplicity (n) as the real event, but there is no requirement that the fake tracks are drawn from events of multiplicity close to n. This is the same procedure as used by DELPHI [12] and allows direct comparison with theoretical calculations. However, it has the consequence that the value of $r(\varepsilon)$ is influenced by the mixing of events with different multiplicities in $\rho_{\rm mix}(\varepsilon)$. For this reason many correlation studies, particularly in hadronic collisions, have used the "semi-inclusive" correlation [10], $r^{(n)}(\varepsilon)$, for which both $\rho(\varepsilon)$ and $\rho_{\rm mix}(\varepsilon)$ are evaluated at a fixed multiplicity n. Monte Carlo studies indicate that, for the data studied in this paper, the difference between $r(\varepsilon)$ and $r^{(n)}(\varepsilon)$ is quite pronounced for low multiplicity ($\langle n(\Theta)\rangle \leq 2$), but largely disappears at high multiplicity.

Analytic calculations for $\hat{r}(\varepsilon)$ and $r(\varepsilon)$, performed in the DLA at asymptotic energies, can be expressed in the form [18]:

$$\hat{Y} \equiv -\frac{\ln(\hat{r}(\varepsilon)/b)}{2\sqrt{\ln(P\sin\Theta/\Lambda)}} \simeq 2\beta(1-0.5\omega(\varepsilon)), \qquad (4)$$

$$Y \equiv \frac{\ln r(\varepsilon)}{\sqrt{\ln(P\sin\Theta/\Lambda)}} \simeq 2\beta(\omega(\varepsilon)-2\sqrt{1-\varepsilon}), \qquad (5)$$

where

$$\omega(\varepsilon) = 2\sqrt{1-\varepsilon}\,(1-\ln(1-\varepsilon)/8)\,, \qquad (6)$$

and β and b are given by

$$\beta = 6(11\,N_c - 2n_f)^{-1/2}, \qquad b = 2\beta\sqrt{\ln(P\sin\Theta/\Lambda)} \quad (7)$$

with $N_c = 3$. The effective number of flavours, n_f, is chosen to be three since the main contribution to the current-region parton cascade comes from light quarks [33]. These values of N_c and n_f give $\beta = 1.15$.

The analytic QCD calculations predict a scaling behaviour, i.e. $\hat{Y}$ and Y are functions of ε only and depend neither on the initial parton momentum $P = Q/2$ nor on the angle Θ. According to the calculations, both $\hat{Y}(\varepsilon)$ and $Y(\varepsilon)$ rise with increasing ε. The increase of $\hat{Y}(\varepsilon)$ determines the behaviour of $\hat{r}(\varepsilon)$, which is a strongly decreasing function due to the decrease in the number of partons (and, hence, parton pairs) with increasing ε (decreasing θ_{12}). In contrast, $r(\varepsilon)$ is predicted to rise with increasing ε, reflecting an increased sensitivity of $r(\varepsilon)$ to two-particle correlations. At large particle separation, i.e. $\theta_{12} \geq \Theta$ ($\varepsilon \leq 0$), there are no two-particle correlations, $r(\varepsilon \leq 0) = 1$ [1].

[1] This statement follows from the analytic DLA calculation, which takes into account the angular ordering but neglects momentum conservation in the gluon splitting. On the other hand, Monte Carlo models which incorporate momentum conservation exhibit long-range two-particle correlations in this phase-space region [18].

2.3 Current-target correlations

A simple way to measure the interdependence between the number of charged particles in the current and target regions, $n_{\rm c}$ and $n_{\rm t}$, is to use the correlation coefficient κ:

$$\kappa = \sigma_{\rm c}^{-1}\sigma_{\rm t}^{-1}{\rm cov}(n_{\rm c}, n_{\rm t}),$$
$${\rm cov}(n_{\rm c}, n_{\rm t}) = \langle n_{\rm c} n_{\rm t}\rangle - \langle n_{\rm c}\rangle\langle n_{\rm t}\rangle, \qquad (8)$$

where $\sigma_{\rm c}$ and $\sigma_{\rm t}$ are the standard deviations of the multiplicity distributions in the current and target regions, respectively. For positive correlations, κ is positive; for anti-correlations it is negative. The advantages of using definition (8) lie in the simplicity of the boundary conditions, $-1 \leq \kappa \leq 1$, which allows a quantitative estimate of the strength of the correlations, and its low sensitivity to the losses of particles from the proton remnants, which often escape undetected down the beam pipe. The latter property comes from the fact that ${\rm cov}(n_{\rm c}, n_{\rm t})$ and the product $\sigma_{\rm c}\,\sigma_{\rm t}$ have a similar dependence on the total number of measured tracks, so that their ratio has only a small dependence on the average track multiplicity in the target region (see Sect. 6).

If hadronisation effects are neglected, the QCDC and BGF processes lead to [29]

$${\rm cov}(n_{\rm c}, n_{\rm t}) \simeq -A_1(Q^2)R_1(Q^2,x) - A_2(Q^2)R_2(Q^2,x), \quad (9)$$

where $A_1(Q^2)$ and $A_2(Q^2)$ are x-independent functions determined by the multiplicity of the outgoing partons. $R_1(Q^2,x)$ is the probability for back-to-back jet events (i.e. with one jet in the current and one in the target region) and $R_2(Q^2,x)$ is the probability for an event without jet activity in the current region.

At small Q^2, the values of $A_1(Q^2)$ and $A_2(Q^2)$ are positive [29]. This leads to a negative covariance (9) and thus to anti-correlations between the current and the target regions, which can be measured using (8). At asymptotically high Q^2, the value of $A_1(Q^2)$ can be negative. In this case the current-target correlations are not strong and can even be positive.

Note that at small fixed Q^2, ${\rm cov}(n_{\rm c}, n_{\rm t})$ is sensitive to the BGF rate as a function of x which, in turn, depends on the gluon density inside the proton [29].

3 Experimental setup

The data were taken in 1995 at the positron-proton collider HERA with the ZEUS detector. During this period, the energy of the positron beam was $E_e = 27.5\,{\rm GeV}$ and that of the proton beam was 820 GeV. The integrated luminosity used for the present study is $6.4\,{\rm pb}^{-1}$.

ZEUS is a multi-purpose detector described in detail in [34]. Of particular importance in the present study are the central tracking detector and the calorimeter.

The central tracking detector (CTD) is a cylindrical drift chamber with nine superlayers covering the polar angle[2] region $15^\circ < \theta < 164^\circ$ and the radial range 18.2-79.4 cm. Each superlayer consists of eight sense wire layers. The transverse momentum resolution for charged tracks traversing all CTD layers is $\sigma(p_\perp)/p_\perp = 0.0058 p_\perp \oplus 0.0065 \oplus 0.0014/p_\perp$ with $p_\perp$ being the track transverse momentum (in GeV). The single hit efficiency of the CTD is greater than 95%.

The CTD is surrounded by the uranium-scintillator calorimeter which is divided into three parts: forward (FCAL), barrel (BCAL) and rear (RCAL). The calorimeter is longitudinally segmented into electromagnetic (EMC) and hadronic (HAC) sections. The energy resolution of the calorimeter under test beam conditions is $\sigma_E/E = 0.18/\sqrt{E}$ for electrons and $\sigma_E/E = 0.35/\sqrt{E}$ for hadrons (with E in GeV).

4 Data selection

The kinematic variables x and Q^2 can be reconstructed using a variety of methods. In order to determine these variables, we use the measurement of energy and angle of the scattered positron, the double angle and the Jacquet-Blondel methods [35]. These three methods are further denoted by the subscripts e, DA and JB, respectively. In the double angle method, the variables x, Q^2 and y are reconstructed using the angles of the scattered positron and the hadronic energy flow. In the Jacquet-Blondel method, used only in the event selection, the kinematic variables are determined entirely from the hadronic system. The boost vector from the laboratory to the Breit frame is determined using the double angle method, which is less sensitive to systematic uncertainties in the energy measurement than the other methods. In the reconstruction of the Breit frame all charged particles are assumed to have pion masses.

The triggering and online event selections are identical to those used in [36]. To select neutral-current DIS events the following cuts are applied:

- $E_e^{'} \geq 10\,\text{GeV}$, $E_e^{'}$ being the energy of the scattered positron.
- $Q^2_{\text{DA}} \geq 10\,\text{GeV}^2$.
- $35 \leq \delta = \sum E_i(1-\cos\theta_i) \leq 60\,\text{GeV}$, where E_i is the energy of the i^{th} calorimeter cell and θ_i is its polar angle with respect to the beam axis.
- $y_e \leq 0.95$.
- $y_{\text{JB}} \geq 0.04$.
- Z-component of the primary vertex position determined from the tracks fitted to the vertex is in the range $-40 < Z_{\text{vertex}} < 50$ cm.

[2] ZEUS has a right-handed coordinate system in which $X = Y = Z = 0$ is the nominal interaction point. The positive Z-axis is along the direction of the proton beam. The X-axis is horizontal, pointing towards the centre of HERA. The polar angle θ is defined with respect to the positive Z-direction.

Table 1. Numbers of selected events used to study the angular correlations in different Q^2 regions, integrated over all x values. The corresponding uncorrected average values of Q^2 and average charged multiplicity $\langle n\rangle$ in the current region of the Breit frame are also shown. The errors are the combined statistical and systematic uncertainties.

Q^2 (GeV^2) range	$\langle Q^2\rangle\,\text{GeV}^2$	$\langle n\rangle$	No. of events
10-20	14.4 ± 0.5	0.96 ± 0.04	161421
20-100	40 ± 1	1.5 ± 0.1	159453
> 100	320 ± 11	2.9 ± 0.3	31461
> 2000	3737 ± 203	3.9 ± 0.6	456

- A timing cut requiring that the event time measured by the RCAL is consistent with an e^+p interaction.
- The impact point (X, Y) of the scattered positron in the RCAL has to lie outside a square of 32×32 cm^2, centred on the beam axis.

About 350k events satisfy the above cuts. Tables 1 and 2 give the numbers of selected events for the kinematic regions used in this analysis.

The present study is based on the CTD tracks fitted to the vertex. The scattered positron was removed from the track sample. In addition, the following cuts to select tracks were imposed:

- Transverse momentum $p_\perp > 150$ MeV.
- $|\ \eta\ | < 1.75$, where η is the pseudorapidity given by $-\ln(\tan(\theta/2))$ with θ being the polar angle of the charged track.

These cuts restrict our study to a well-understood, high-acceptance region of the CTD.

To understand the uncertainties in our results, a subsample of DIS events containing a single jet was selected using calorimeter information. The cone algorithm [37] was used with radius $R = \sqrt{\delta\eta^2 + \delta\phi^2} = 1$, where $\delta\eta$ and $\delta\phi$ are the differences of pseudorapidity and azimuthal angles of energy deposits in the calorimeter with respect to the jet direction. Events with a single jet (in addition to particles in the proton remnant) are selected if the jet transverse energy E_T is larger than 4 GeV. The jet pseudorapidity is restricted to the region $|\ \eta_{\text{jet}}\ | < 2$, where jets are well reconstructed. After the transformation to the Breit frame, only jets which belong to the current region of the Breit frame are considered.

5 Event simulation

To determine the corrections for selection and acceptance losses, event migration between (x, Q^2) bins, and track migration between the current and target regions due to mis-reconstruction of the Breit frame, a sample of neutral-current DIS events was generated with ARIADNE 4.8 [38] using tuned parameters [39]. This MC is based on the colour-dipole QCD model supplemented with the Boson-Gluon Fusion process. The hadronisation is described by

Table 2. Bins in Q^2 and x used to study the current-target correlations. The average values of Q^2 and x are shown without detector corrections. The errors are the combined statistical and systematic uncertainties

Q^2 (GeV^2) range	x range	$\langle Q^2 \rangle$ GeV^2	$\langle x \rangle$	No. of events
evolution with Q^2				
10–20	$0.6 - 2.4 \cdot 10^{-3}$	14.2 ± 0.6	$(1.22 \pm 0.01) \cdot 10^{-3}$	79381
20–40	$1.2 - 10 \cdot 10^{-3}$	28.7 ± 0.7	$(2.88 \pm 0.01) \cdot 10^{-3}$	48287
40–80	$1.2 - 10 \cdot 10^{-3}$	55 ± 2	$(3.82 \pm 0.01) \cdot 10^{-3}$	34956
80–160	$2.4 - 10 \cdot 10^{-3}$	109 ± 3	$(5.29 \pm 0.02) \cdot 10^{-3}$	11331
160–320	$2.4 - 50 \cdot 10^{-3}$	218 ± 5	$(2.1 \pm 0.1) \cdot 10^{-2}$	4350
320–640	$10 - 50 \cdot 10^{-3}$	416 ± 9	$(2.4 \pm 0.2) \cdot 10^{-2}$	1615
640–1280	$10 - 50 \cdot 10^{-3}$	899 ± 14	$(1.7 \pm 0.2) \cdot 10^{-2}$	270
evolution with x				
10–1280	$0.6 - 1.2 \cdot 10^{-3}$	20.7 ± 0.4	$(8.7 \pm 0.1) \cdot 10^{-4}$	72039
10–1280	$1.2 - 2.4 \cdot 10^{-3}$	28 ± 2	$(1.7 \pm 0.1) \cdot 10^{-3}$	74621
10–1280	$2.4 - 10 \cdot 10^{-3}$	53 ± 5	$(4.4 \pm 0.1) \cdot 10^{-3}$	73825

the JETSET model [40]. Hadrons with lifetime $c\tau > 1$ cm are treated as stable. The GRV94 HO [41] parameterization of the proton parton distribution functions is used. The MC events obtained by this procedure define the generator-level sample.

For the detector-level sample, the events are generated with ARIADNE using the DJANGO 6.24 [42] program based on HERACLES 4.5.2 [43] in order to incorporate first-order electroweak corrections. The events are then processed through a simulation of the detector using GEANT 3.13 [44] to take into account particle interactions with the detector material, particle decays, event and track migrations, double counting of single tracks, resolution, acceptance of the detector and event selection. The detector-level MC events are processed with the same reconstruction program as used for the real data.

In addition to ARIADNE, the LEPTO 6.5 [45] and HERWIG 5.9 [46] generators with tuned parameters [39] are also used to compare with the data. The parton cascade in LEPTO is based on the matrix element calculation matched to a parton shower (MEPS) according to the DGLAP equation. LEPTO orders the parton emissions in invariant mass with an additional angular constraint to ensure coherence. As in ARIADNE, the hadronisation in LEPTO is described by the JETSET model. HERWIG also has a parton shower based on the DGLAP equation, but parton emissions are ordered in angle. The hadronisation is described by a cluster model.

One of the sources of two-particle correlations is the Bose-Einstein interference between identical particles. By default, this effect is turned off in the JETSET model. The simulation of the Bose-Einstein effect is absent in HERWIG. According to our studies and the DELPHI results [12], the Bose-Einstein interference has a small effect (less than 2% of relative change) on the angular correlations.

6 Resolution and acceptance

For the present analysis, it is important to understand the two-particle resolution of the CTD. The resolution is determined in the Breit frame as the variance of the absolute difference between θ_{12} measured at the generator-level and the detector-level Monte Carlo defined above. It is found that to ensure that the two particles are resolved, the angle θ_{12} between two tracks in the current region of the Breit frame should not be smaller than two degrees. For a given Θ, P and Λ, this limit determines the maximum values of ε used in this analysis.

For the cuts used, the event and current-region track acceptances are both in the range $70 - 90\%$, depending on the (Q^2, x) region studied. This is sufficiently good to measure the angular correlations reliably.

For the target region, the track acceptance lies in the range $20 - 30\%$. The low acceptance results mainly from the $|\ \eta\ | < 1.75$ restriction. Using the ARIADNE model, the low target-region acceptance is found to have a small effect on the current-target correlations measured according to (8): the restriction $|\ \eta\ | < 1.75$ decreases the absolute value of $\mathrm{cov}(n_\mathrm{c}, n_\mathrm{t})$ by 50%. However, this decrease is compensated partially in κ by a similar decrease in the standard deviations of (8). As a result, the cut $|\ \eta\ | < 1.75$ decreases the absolute value of κ by only 15%.

If the average charged multiplicity $\langle n_\mathrm{t} \rangle$ is measured in the target region as a function of the multiplicity n_c in the current region, the restriction $|\ \eta\ | < 1.75$ decreases the $\langle n_\mathrm{t} \rangle$ by a factor of 2 to 5, depending on n_c. Therefore, for the present target-region acceptance, the average number of particles in the target region as a function of the multiplicity in the current region (or vice versa) cannot be reliably determined, which is why κ is used, as described in Sect. 2.3.

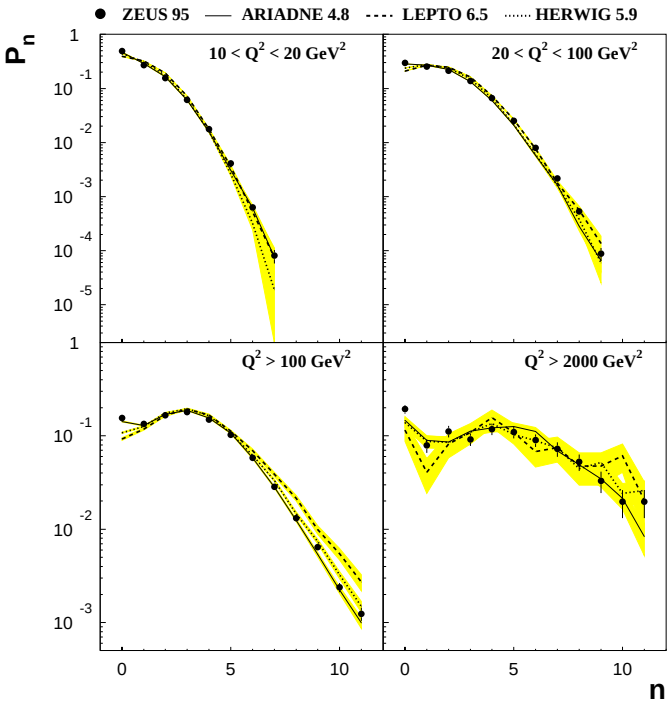

Fig. 2. Probability distribution P_n for detecting n charged particles in the current region of the Breit frame for different ranges of Q^2. The uncorrected data are compared to MC predictions after the detector simulation. The errors on the data are the statistical uncertainties. The shaded bands show the statistical uncertainties on the MC predictions. Table 3 gives the χ^2/NDF of the MC predictions

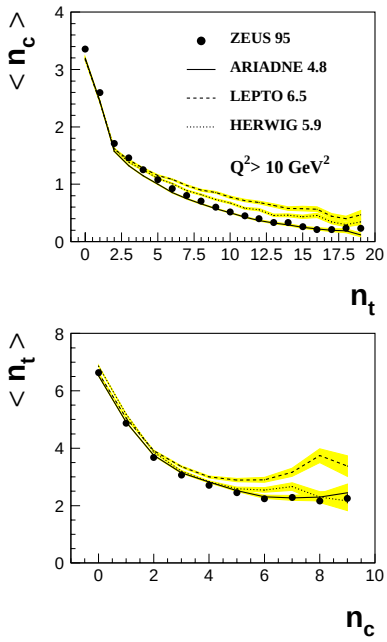

Fig. 3. Average charged multiplicities in the current (target) hemisphere as a function of the multiplicity in the opposite hemisphere for $Q^2 > 10\,\mathrm{GeV}^2$. The uncorrected data are compared to MC predictions after the detector simulation. The statistical uncertainties on the data are typically smaller than the size of the symbols. The shaded bands show the statistical uncertainties on the MC predictions

Table 3. $\chi^2 = \sum_i \left(P_n^{\mathrm{Data}} - P_n^{\mathrm{MC}}\right)^2 / (\sigma^2_{\mathrm{Data}} + \sigma^2_{\mathrm{MC}})$ per degree of freedom for the uncorrected probability distribution P_n shown in Fig. 2

Q^2 (GeV^2) range	χ^2/NDF		
	ARIADNE 4.8	LEPTO 6.5	HERWIG 5.9
10-20	25.4	189.6	73.8
20-100	27.7	167.9	71.1
> 100	4.5	34.3	32.9
> 2000	1.0	1.3	0.9

7 Uncorrected observables

To understand how well the MC models describe simple observables related to the angular and current-target correlations, we compare the uncorrected data to the MC distributions after the detector simulation. Table 1 gives the numbers of events in each region of Q^2, the average values of Q^2 and the average charged multiplicity in the current region of the Breit frame for the data.

Fig. 2 shows the probability, P_n, of detecting n charged particles in the current region of the Breit frame for four Q^2 regions. The difference between the data and Monte Carlo models is illustrated by the χ^2/NDF in Table 3. Note that, although the angular correlations are sensitive to P_n, they are also determined by the semi-inclusive two-particle densities [10].

The average charged multiplicities in the current (target) hemisphere as a function of the multiplicity in the opposite hemisphere are shown for $Q^2 > 10\,\mathrm{GeV}^2$ in Fig. 3. In both cases the average multiplicity in a hemisphere decreases as the number of particles in the opposite hemisphere increases, which is a signature of anti-correlations between current and target charged multiplicities.

These comparisons show that ARIADNE gives the best description of the uncorrected observables. Therefore, this model is used to correct the correlations for detector effects.

8 Correction procedure

Due to the complexity of the measured variables, a bin-by-bin correction procedure is used. The correction factors $\mathcal{C}$ for each kinematic region in (Q^2, x) are evaluated separately for each observable, $\mathcal{A} = \hat{r}(\varepsilon), r(\varepsilon), \kappa$,

$$\mathcal{C} = \frac{\mathcal{A}^{\mathrm{gen}}}{\mathcal{A}^{\mathrm{det}}}, \tag{10}$$

where $\mathcal{A}^{\mathrm{gen}}$ is calculated at the generator-level of ARIADNE and $\mathcal{A}^{\mathrm{det}}$ is that at the detector-level of this model. The corrected value for an observable is found by multiplying its measured value by the relevant correction factor.

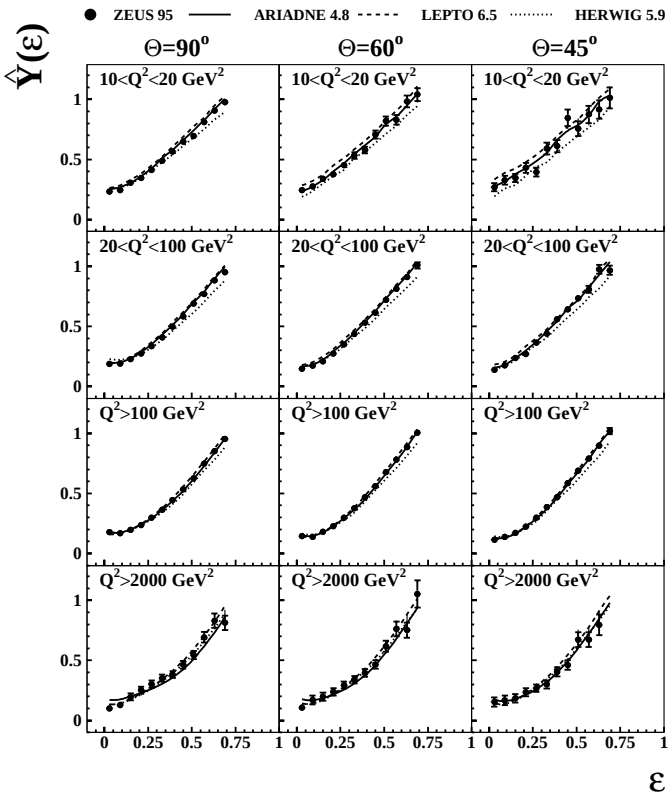

Fig. 4. The normalised particle density $\hat{Y}(\varepsilon)$ in the current region for four Q^2 ranges and three different Θ values compared to MC predictions. The rescaling is performed using $\Lambda = 0.15\,\mathrm{GeV}$. The inner bars on the corrected data show the statistical uncertainties. The full error bars include the systematic uncertainties, which are typically negligible compared to the statistical errors

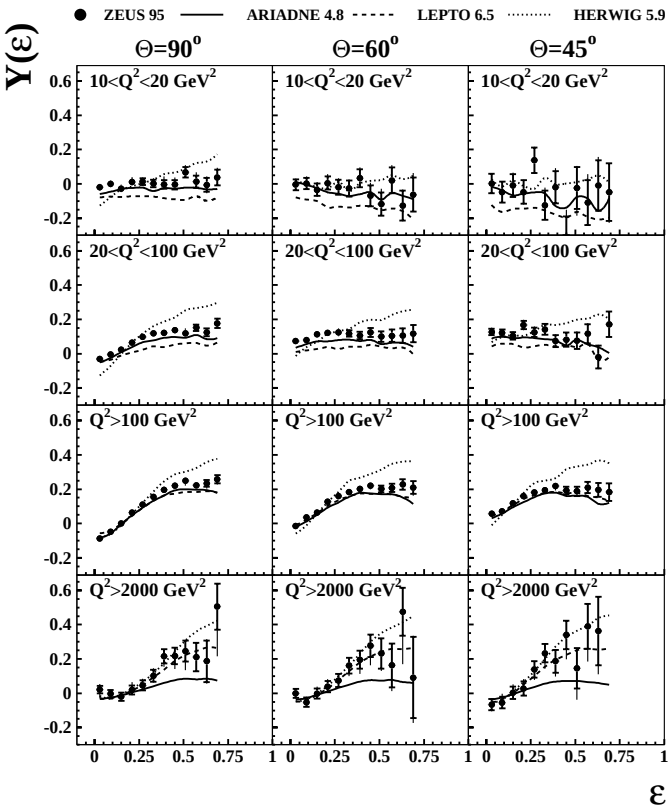

Fig. 5. The correlation function $Y(\varepsilon)$ in the current region for four Q^2 ranges and three different Θ values compared to MC predictions. The rescaling was performed using $\Lambda = 0.15\,\mathrm{GeV}$. The inner error bars on the corrected data show the statistical uncertainties and the full error bars include the systematic uncertainties

The correction factors are close to unity for all observables and vary smoothly for any given $\mathcal{A}$. For $\hat{r}(\varepsilon)$ and $r(\varepsilon)$, the correction factors are never larger than 1.3 and decrease with increasing ε. For the current-target correlations, the correction factors never exceed 1.35. The sign of these correlations remains unchanged after the correction procedure.

9 Statistical and systematic uncertainties

The main sources of systematic uncertainties are:

- Event reconstruction and selection. The systematic check was performed by varying the cuts on y_e, y_{JB}, δ and the vertex position requirement ($y_e \leq 0.90$, $y_{\mathrm{JB}} \geq 0.05$, $40 \leq \delta \leq 55\,\mathrm{GeV}$, $-35 < Z_{\mathrm{vertex}} < 45\,\mathrm{cm}$). The contribution of these uncertainties for the angular and current-target correlations is typically 60% of the total systematic errors.
- Track reconstruction and selection. The cuts were tightened: tracks should have transverse momenta larger than 200 MeV and $|\,\eta\,| < 1.5$. Tracks which reach at least the third CTD superlayer were used. These uncertainties are typically 30% of the total systematic errors.
- The use of tracks not fitted to the primary vertex.

The overall systematic uncertainty is determined by adding the uncertainties discussed above in quadrature. The error bars on the corrected data presented in Sect. 10 include both statistical and systematic errors added in quadrature. The errors on the angular correlations are dominated by the statistical errors (about $80 - 90\%$ of the total error). For the current-target correlations, the major uncertainty comes from the systematic effects.

No systematic uncertainty is attributed to the use of LEPTO or HERWIG in place of ARIADNE to determine the correction factors, since these models do not adequately describe the raw data for several variables relevant to the correlation study. If the difference between the correction factors determined using ARIADNE and those using LEPTO or HERWIG is added, the systematic errors increase by about 50%.

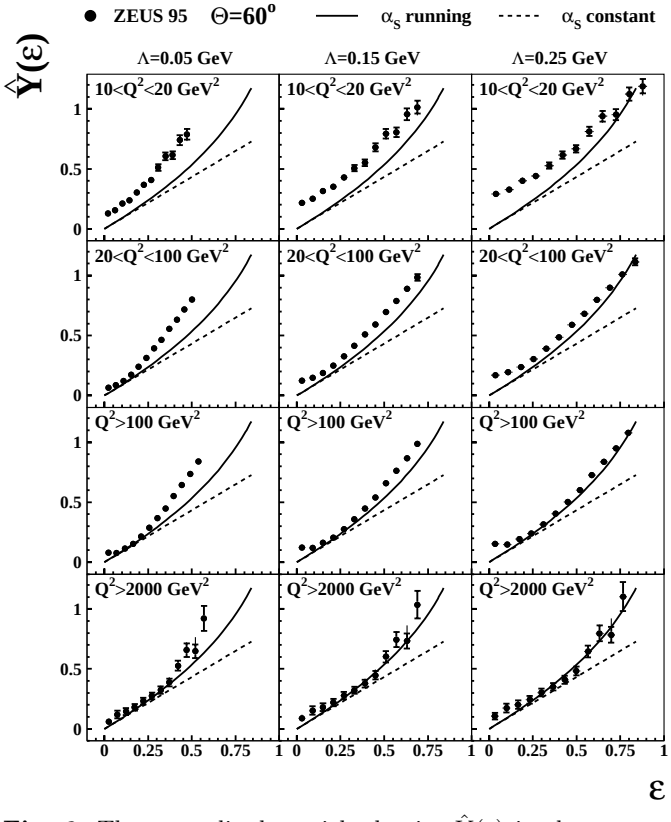

Fig. 6. The normalised particle density $\hat{Y}(\varepsilon)$ in the current region for $\Theta = 60^\circ$ compared to the analytic QCD predictions (4) for different effective Λ values. Solid (dashed) lines show the predictions at asymptotic energy for a running (fixed) coupling constant

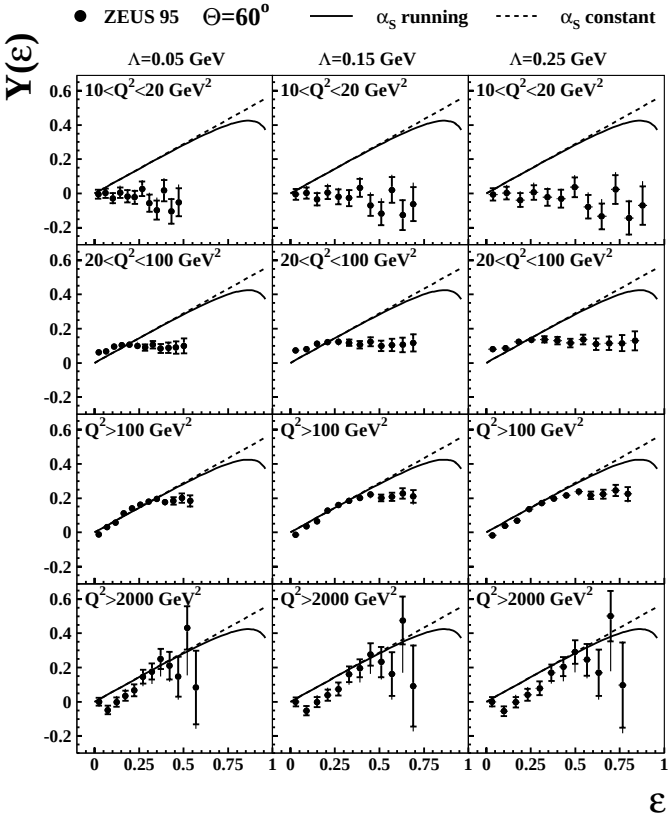

Fig. 7. The correlation function $Y(\varepsilon)$ in the current region for $\Theta = 60^\circ$ compared to the analytic QCD predictions (5) for different effective Λ values. Solid (dashed) lines show the predictions at asymptotic energy for a running (fixed) coupling constant

10 Results

10.1 Two-Particle angular correlations

The behaviour of the normalised particle density, $\hat{Y}(\varepsilon)$, (see (4)) and correlation function, $Y(\varepsilon)$, (see (5)), measured in the four Q^2 regions, listed in Table 1, are shown in Figs. 4 and 5 for three values of Θ. For these figures, the value of $\Lambda = 0.15\,\mathrm{GeV}$ was chosen in order to be consistent with similar measurements made at LEP [12,13].

The values of $\hat{Y}(\varepsilon)$ increase with increasing ε, reflecting a strong decrease of the number of particle pairs with increase of ε. Such a trend is mostly determined by the single-particle distribution, rather than correlations between particles. In contrast, $Y(\varepsilon)$ is more sensitive to two-particle correlations. It rises with increasing ε at large Q^2, where the particle multiplicity is larger and the jet structure is more pronounced. This behaviour implies an increase in the strength of the correlations with decreasing angular separation between the two particles. At low Q^2, however, this rise is not observed due to the small charged particle multiplicity in the current region.

The $\hat{Y}(\varepsilon)$ distributions of the MC models agree reasonably well with the data. The ARIADNE model describes the data in all Q^2 regions. At low Q^2, LEPTO slightly overestimates $\hat{Y}(\varepsilon)$, while HERWIG underestimates it. The agreement is less satisfactory for $Y(\varepsilon)$. ARIADNE is quite successful in the description of low and medium Q^2, but underestimates the data at high Q^2. LEPTO fails to describe the data at $Q^2 \leq 100\,\mathrm{GeV}^2$. HERWIG gives a poor description of $Y(\varepsilon)$ in all Q^2 regions, except for the highest Q^2.

In the current version of ARIADNE 4.8, the suppression of available phase space for parton radiation due to the extended nature of the target remnant can also affect the current region of the Breit frame at high Q^2. A recent (as yet unreleased) modification of ARIADNE [47], which ensures that the whole of the available current-region phase space is used for gluon radiation, gives a good description of $Y(\varepsilon)$ at high Q^2 (not shown).

The results indicate that there are no changes in the $\hat{Y}(\varepsilon)$ and $Y(\varepsilon)$ distributions at large ε as the angle Θ is varied in the range from 45° to 90°. This observation supports the predicted scaling property of (4) and (5). To compare the analytic calculations with the data, we choose $\Theta = 60^\circ$. Figure 6 shows $\hat{Y}(\varepsilon)$ and the asymptotic QCD predictions (4) for fixed (dashed lines) and running (solid

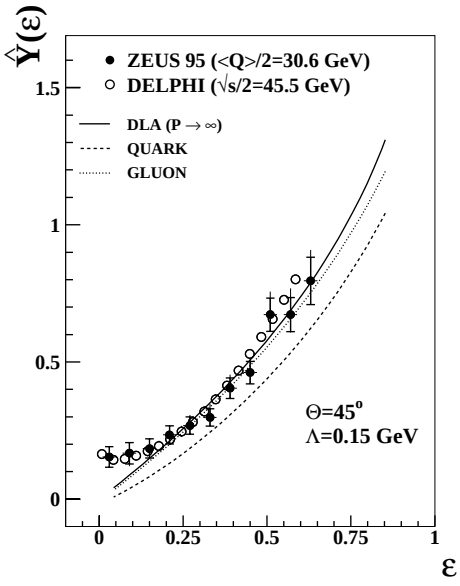

Fig. 8. The normalised particle density $\hat{Y}(\varepsilon)$ for $Q^2 > 2000\,\mathrm{GeV}^2$ ($P = \langle Q\rangle/2 = 30.6\,\mathrm{GeV}$) compared to the analytic QCD predictions and DELPHI results for $P = 45.5\,\mathrm{GeV}$. For both experiments $\Theta = 45^\circ$ and $\Lambda = 0.15\,\mathrm{GeV}$. The solid line shows the DLA predictions at asymptotic energy for a running coupling constant. The dashed (dotted) line corresponds to the prediction at finite energy ($P = 30.6\,\mathrm{GeV}$) for quark (gluon) jets

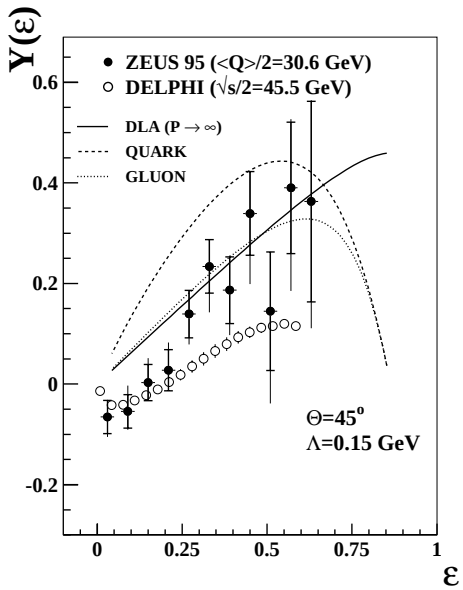

Fig. 9. The correlation function $Y(\varepsilon)$ for $Q^2 > 2000\,\mathrm{GeV}^2$ ($P = \langle Q\rangle/2 = 30.6\,\mathrm{GeV}$) compared to the analytic QCD predictions and DELPHI results for $P = 45.5\,\mathrm{GeV}$. For both experiments, $\Theta = 45^\circ$ and $\Lambda = 0.15\,\mathrm{GeV}$. The solid line shows the DLA predictions at asymptotic energy for a running coupling constant. The dashed (dotted) line corresponds to the prediction at finite energy ($P = 30.6\,\mathrm{GeV}$) for quark (gluon) jets

lines) strong coupling constant[3] for three different values of Λ. For the calculations with a fixed coupling constant, the values $\Lambda = 0.05, 0.15, 0.25\,\mathrm{GeV}$ for $Q^2 > 2000\,\mathrm{GeV}^2$ correspond to the effective $\alpha_s = 0.107, 0.130, 0.144$ for the lowest-order QCD relation between the α_s and Λ. The assumption of a fixed coupling constant is inconsistent with the data for all Q^2 intervals, while the calculation with a running coupling constant shows reasonable agreement with the data at $Q^2 > 2000\,\mathrm{GeV}^2$ and large Λ.

A similar comparison of the analytic calculations for $Y(\varepsilon)$ with the data is shown in Fig. 7. As for $\hat{Y}(\varepsilon)$, discrepancies are observed at small Q^2. The agreement is better at high Q^2; however, the calculations still overestimate the data at small ε. This discrepancy is likely to be related to the neglect of energy-momentum conservation in the DLA, as recently discussed in [12,13]. This simplification makes the angular correlations in the analytic calculations more prominent for large angular separations, θ_{12} (small ε).

Figs. 8 and 9 show our results for $\hat{Y}(\varepsilon)$ and $Y(\varepsilon)$ at $\Theta = 45^\circ$ and $\Lambda = 0.15\,\mathrm{GeV}$ together with the DELPHI data at $P = 45.5\,\mathrm{GeV}$ ($\sqrt{s} = 91\,\mathrm{GeV}$) [12]. The ZEUS data are shown for $Q^2 > 2000\,\mathrm{GeV}^2$, which corresponds approximately to $P = \langle Q\rangle/2 = 30.6\,\mathrm{GeV}$. Despite the difference in energy, the results for $\hat{Y}(\varepsilon)$ agree. Note that no significant energy dependence of $\hat{Y}(\varepsilon)$ was found at LEP [12].

According to [12], the behaviour of $Y(\varepsilon)$ at $\sqrt{s} = 183\,\mathrm{GeV}$ is steeper than that at $\sqrt{s} = 91\,\mathrm{GeV}$. If there is a universality between the current region of DIS and a single hemisphere of e^+e^-, one might expect that e^+p data at $P = \langle Q\rangle/2 = 30.6\,\mathrm{GeV}$ should exhibit a less strong rise than e^+e^- data at $P = 45.5\,\mathrm{GeV}$. However, the ZEUS data shown in Fig. 9 exhibit the opposite trend, which suggests differences between the angular correlations in the current region of DIS and a single hemisphere of e^+e^- annihilation. The observed discrepancy might be related to different choices of the axis of the Θ-cone: whereas this axis in e^+e^- was determined by the sphericity axis, the virtual photon direction is used to determine the axis of the Θ-cone in DIS. In addition, the leading-order QCD effects discussed in Sect. 2 can lead to an uncertainty in our results. To investigate this issue, similar studies of the angular correlations were performed using only single-jet events. The single-jet pre-selection described in Sect. 4 leads to smaller values of $Y(\varepsilon)$ than the data shown in Fig. 9, but a small discrepancy with e^+e^- still remains.

Several further checks have been performed to understand the difference between the ZEUS and the DELPHI results for $Y(\varepsilon)$. Firstly, $\ln(P\Theta/\Lambda)$ was used in the denominator of (1), as in the DELPHI analysis. Secondly, a small fraction of events at $Q^2 > 8000\,\mathrm{GeV}^2$ was rejected, so that no event has an initial parton at an energy higher than $P = 45.5\,\mathrm{GeV}$. The analysis was repeated by calcu-

[3] An evolution of the parton shower at a *fixed* energy scale Q^2 is characterized by a running coupling constant, α_s, which reflects a change of energy scale as the parton shower evolves.

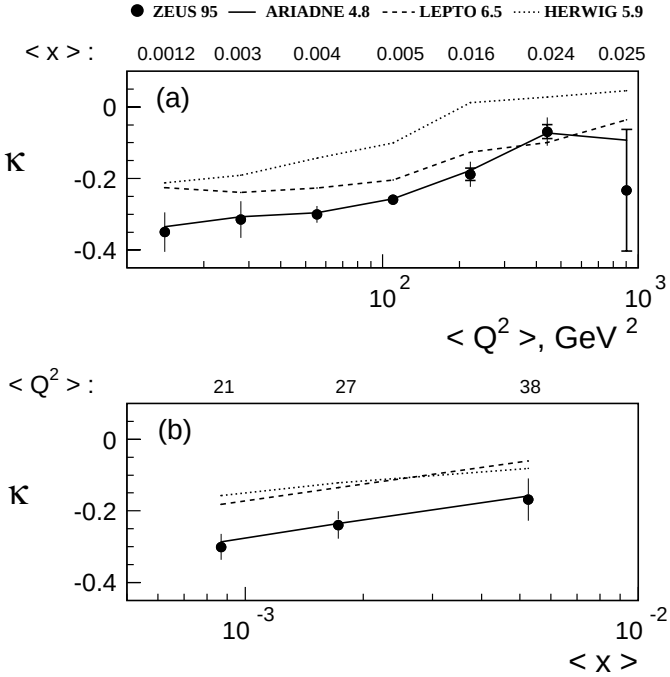

Fig. 10. a represents the evolution of the coefficient of correlations κ with predominant variation in Q^2 for corrected data and MC predictions; **b** shows the same quantity where predominantly x varies. The corrected values of $\langle Q^2 \rangle$ and $\langle x \rangle$ are indicated for each plot. The inner error bars on the data show the statistical uncertainties. The full error bars include the systematic uncertainties

lating ε with $P = \sqrt{\langle Q^2 \rangle}/2$, rather than using $P = Q/2$ for each individual event. In addition, HERWIG and the modified version of ARIADNE without the suppression effect in the current region were used. Both models describe $Y(\varepsilon)$ at $Q^2 > 2000\,\mathrm{GeV}^2$, and, therefore, they are better suited to correct the data in this region. For the checks discussed above, no significant changes in the ZEUS data were observed which can account for the discrepancy.

Figs. 8 and 9 also show the analytic QCD results [18] at infinite energy and finite energy ($P = 30.6\,\mathrm{GeV}$) separately for quark and gluon jets. The analytic prediction for gluon jets shows better agreement with the data than that for quark jets. However, it again fails to describe $Y(\varepsilon)$ at small ε. A possible source of the discrepancy with the finite-energy quark prediction is the ratio $R = 9/4$ of the mean parton multiplicity in gluon and quark jets used in the calculations for quark jets. If one goes beyond the DLA, the value of this ratio is smaller than 9/4. For example, in the next-to-leading log approximation, $R \simeq 1.8$ [48]. A smaller value of R will bring the analytic prediction for quark jets closer to the gluon prediction [32].

10.2 Current-Target correlations

Figure 10 shows the behaviour of the correlation coefficient κ as a function of the average values of Q^2 and x. The same bins in Q^2 and x were used as in previous studies [1,2]. Instead of calculating κ in each bin, the bins are combined to increase the statistics. Table 2 gives the numbers of events and the uncorrected average values of Q^2 and x. Fig. 10a shows the dependence of the correlations on Q^2, while Fig. 10b shows the x variation. Note that the average values of Q^2 and x shown in the figure are corrected.

Anti-correlations ($\kappa < 0$) are observed for all values of x and Q^2, as predicted by (9). The magnitude of κ decreases with increasing $\langle Q^2 \rangle$ from 0.35 to 0.1. According to the analytic result of (9), the observed anti-correlations can be due to the $\mathcal{O}(\alpha_s)$ effects (QCDC and BGF). Their kinematics in the Breit frame can reduce the particle multiplicity in the current region and increase it in the target region. A Monte Carlo study [29] shows that the contribution from hadronisation is relatively small.

The ZEUS result, shown in Fig. 10, gives a quantitative estimate of the correlations between the current and target region multiplicities in DIS at HERA, an effect which is quite different from that observed between the forward and backward hemisphers in e^+e^- annihilation [21, 23–25]. The kinematics of the $\mathcal{O}(\alpha_s)$ effects in the Breit frame that lead to these correlations are also a possible source of the disagreement between ZEUS and e^+e^- data for the angular correlations. These effects can also lead to discrepancies between the data and the analytic QCD calculations which do not take into account the kinematics of the $\mathcal{O}(\alpha_s)$ processes in the Breit frame. It is noteworthy that the current region of DIS shows a different average multiplicity at small Q^2 than a single hemisphere of e^+e^- annihilation [1,3,4] due to the $\mathcal{O}(\alpha_s)$ processes.

The magnitude of the anti-correlations increases with decreasing $\langle x \rangle$. According to the analytic result (9), this can be due to an increase of the fraction of events with one or two jets produced in the target region. This behaviour is driven by an increase of the gluon density inside the proton, leading to an increase of the Boson-Gluon Fusion rate.

The ARIADNE model agrees well with the data. A reasonable description of dijet production in DIS by this model [49] is possibly responsible for this agreement. The LEPTO and HERWIG predictions show the same trend but do not reproduce the magnitude of the correlations, which is likely to be related to a lower predicted dijet rate [49].

11 Conclusions

The evolution of two-particle angular correlations with Q^2 of DIS has been studied in the Breit frame. The data have been compared to the results of numerical simulations and to those of analytic QCD calculations in the DLA for partons, assuming the Local Parton-Hadron Duality hypothesis.

The results on the angular correlations support the predicted scaling behaviour in the angle Θ at large ε. The scaling in energy is found to hold approximately for $\hat{Y}(\varepsilon)$.

For this variable, our results are in good agreement with those of DELPHI for e^+e^-, despite the difference in the energy. In contrast to $\hat{Y}(\varepsilon)$, the two-particle correlation function $Y(\varepsilon)$ depends strongly on Q^2: at low Q^2, the two-particle correlations are suppressed, but they increase with ε at high Q^2 ($Q^2 > 100\,\mathrm{GeV}^2$).

The analytic calculations for $\hat{Y}(\varepsilon)$ and $Y(\varepsilon)$ do not describe the data at low Q^2. The results become closer to the data as Q^2 increases. The asymptotic QCD predictions with a running coupling constant only describe the $\hat{Y}(\varepsilon)$ at $Q^2 > 100\,\mathrm{GeV}^2$ for large values of the effective Λ. For the highest Q^2 studied, the predictions reproduce the trend of $Y(\varepsilon)$ but overestimate the data at small ε.

The best description of the angular correlations is achieved by the ARIADNE model, although it fails to describe $Y(\varepsilon)$ at the highest Q^2 studied. The prediction of ARIADNE shows smaller correlations in this region than the data due to the suppression of available current-region phase space by the remnant in the colour-dipole model. LEPTO and HERWIG show small discrepancies for $\hat{Y}(\varepsilon)$. For the $Y(\varepsilon)$ distribution, which is more sensitive to the two-particle correlations, both models fail to describe the data at low Q^2.

The current-target correlations in the Breit frame are found to be large and negative. They are thus very different from those measured in e^+e^- collisions, where small and positive forward-backward correlations have been observed. In DIS, the correlations increase with decreasing x. Such a behaviour is expected from an increase of the Boson-Gluon Fusion rate that leads to an increase of dijet production. ARIADNE agrees well with the current-target correlations. Neither LEPTO nor HERWIG reproduce the magnitude of the correlations. Insufficient dijet production in these models is a possible source of this failure.

Many studies at HERA have found similarity between multiparticle production in the current region of e^+p collisions and a single hemisphere of e^+e^- annihilation. This paper demonstrates that correlations are a powerful tool for investigating this area. For high Q^2, the ZEUS results show differences between the two-particle angular correlations in DIS and e^+e^- annihilation; this is inconsistent with the universality of two-particle inclusive densities, which are expected to be sensitive to the kinematics of the first-order QCD processes producing final-state hadrons in both the current and target regions.

Acknowledgements. This paper was completed shortly after the tragic and untimely death of Prof. Dr. B. H. Wiik. All members of the ZEUS Collaboration wish to acknowledge the tremendous role which he played in the success of the HERA project and this experiment. His leadership and friendship will be greatly missed. We wish to express our gratitude to the DESY accelerator division for the excellent performance of the HERA machine. We acknowledge the effort of all engineers and technicians who have participated in the construction and maintenance of the ZEUS experiment. The support and encouragement of the DESY directorate continues to be invaluable for the work of the ZEUS collaboration. We thank B. Buschbeck, W. Kittel, W. Metzger, W. Ochs and J. Wosiek for helpful discussions.

References

1. ZEUS Collaboration, M. Derrick et al., Z. Phys. C67 (1995) 93.
2. ZEUS Collaboration, J. Breitweg et al., Phys. Lett. B414 (1997) 428.
3. H1 Collaboration, C. Adloff et al., Nucl. Phys. B504 (1997) 3.
4. ZEUS Collaboration, J. Breitweg et al., DESY 99-041 (submitted to Eur. Phys. J. C).
5. ZEUS Collaboration, M. Derrick et al., Z. Phys. C70 (1996) 1.
6. H1 Collaboration, C. Adloff et al., Nucl. Phys. B485 (1997) 3.
7. H1 Collaboration, S. Aid et al., Z. Phys. C72 (1996) 573.
8. H1 Collaboration, C. Adloff et al., Z. Phys C75 (1997) 437.
9. H1 Collaboration, C. Adloff et al., Eur. Phys. J. C5 (1998) 439.
10. E.A. De Wolf, I.M. Dremin and W. Kittel, Phys. Rep. 270 (1996) 1.
11. H1 Collaboration, S. Aid et al., Z. Phys. C72 (1996) 573.
12. DELPHI Collaboration, P. Abreu et al., Phys. Lett. B440 (1998) 203.
13. L3 Collaboration, M. Acciarri et al., Phys. Lett. B428 (1998) 186; B429 (1998) 375.
14. OPAL Collaboration, G. Abbiendi et al., CERN-EP/99-009 (submitted to Eur. Phys. J. C).
15. Yu. Dokshitzer, V.A. Khoze, S.I. Troyan and A.H. Mueller, Rev. Mod. Phys. 60 (1988) 373; Yu.L. Dokshitzer, V.A. Khoze, A.H. Mueller and S.I. Troyan, "Basics of Perturbative QCD", Editions Frontières, 1991.
16. V.A. Khoze and W. Ochs, Int. J. Mod. Phys. A12 (1997) 2949.
17. Ya.I. Azimov, Yu.L. Dokshitzer, V.A. Khoze and S.I. Troyan, Z. Phys. C27 (1985) 65; C31 (1986) 213.
18. W. Ochs and J. Wosiek, Phys. Lett. B289 (1992) 159; B304 (1993) 144; Z. Phys. C68 (1995) 269.
19. Yu. Dokshitzer and I.M. Dremin, Nucl. Phys. B402 (1993) 139.
20. Ph. Brax, J.-L. Meunier and R. Peschanski, Z. Phys. C62 (1994) 649.
21. TASSO Collaboration, M. Althoff et al., Z. Phys. C29 (1985) 347; TASSO Collaboration, W. Braunschweig et al., Z. Phys. C45 (1989) 193 ; HRS Collaboration, M. Derrick et al., Phys. Rev. D34 (1986) 3304; Z. Phys. C35 (1987) 323.
22. EMC Collaboration, M. Arneodo et al., Nucl. Phys. B258 (1985) 249.
23. DELPHI Collaboration, P. Abreu et al., Z. Phys. C50 (1991) 185.
24. Y.G. Xie (for the ALEPH Collaboration,), XXI Int. Symp. on Multiparticle Dynamics, Wuhan, China, 1991, Ed. W. Yuanfong, L. Lianshou, (World Scientific, Singapore, 1992) p.172.
25. OPAL Collaboration, R. Akers et al., Phys. Lett. B320 (1994) 417; M. Cuffiani (for the OPAL Collaboration,) XXIV Int. Symp. on Multiparticle Dynamics, Vietri sul Mare, Selerno, Italy, 1994, Ed. A. Giovannini et al., (World Scientific, Singapore, 1995) p.37.

26. H. Grässler et al., Nucl. Phys. B223 (1983) 269.
27. T. Kafka et al., Phys. Rev. Lett. 34 (1975) 687; S. Uhlig et al., Nucl. Phys. B132 (1978) 15; K. Alpgard et al., Phys. Lett. B123 (1983) 601; G.J. Alner et al., Nucl. Phys. B291 (1987) 445; R.E. Ansorge et al., Z. Phys. C37 (1988) 191.
28. NA22 Collaboration, V.V. Aivazyan et al., Z. Phys. C42 (1989) 533.
29. S.V. Chekanov, J. Phys. G25 (1999) 59; S.V. Chekanov, Presented at XXVIII International Symposium on Multiparticle Dynamics, 1998, (Delphi, Greece) hep-ph/9810477.
30. R.P. Feynman, "Photon-Hadron Interactions", Benjamin, New York, 1972.
31. K.H. Streng, T.F. Walsh and P.M. Zerwas, Z. Phys. C2 (1979) 237.
32. W. Ochs, private communication.
33. S. Lupia and W. Ochs, Phys. Lett. B365 (1996) 339.
34. ZEUS Collaboration, M. Derrick et al., Phys. Lett. B293 (1992) 465; Z. Phys. C63 (1994) 391.
35. F. Jacquet and A. Blondel, Proc. of the study for an *ep* facility for Europe, DESY 79-48 (1979) 391; U. Amaldi et al., DESY 79-48 (1979) 377; S. Bentvelsen, J. Engelen and P. Kooijman, Proc. of the 1991 Workshop on Physics at HERA, DESY Vol.1, Ed. W. Buchmüller and G. Ingelman, (1992) p.23.
36. ZEUS Collaboration, M. Derrick et al., Z. Phys. C72 (1996) 399.
37. J. Huth et al., Proc. of the 1990 DPF Summer Study on High Energy Physics, Snowmass, Colorado, Ed. E.L. Berger, (World Scientific, Singapore, 1992) 134; CDF Collaboration, F. Abe et al., Phys. Rev. D45 (1992) 1448.
38. ARIADNE 4.07, L. Lönnblad, Comp. Phys. Commun. 71 (1992) 15.
39. N.H. Brook et al., Proc. of the Workshop 1995/1996 *Future Physics at HERA*, DESY, Ed. G. Ingelman et al., (1996) p.613.
40. PYTHIA 5.7 and JETSET 7.4, T. Sjöstrand, Comp. Phys. Commun. 82 (1994) 74.
41. M. Glück, E. Reya and A. Vogt, Phys. Lett. B306 (1993) 391.
42. DJANGO 6.24, K. Charchuła, G.A. Schuler, H. Spiesberger, Comp. Phys. Commun. 81 (1994) 381.
43. HERACLES 4.5.2, A. Kwiatkowski, H.-J. Möhring, H. Spiesberger, Comp. Phys. Commun. 69 (1992) 155.
44. GEANT3, R. Brun et al., CERN DD/EE/84-1 (1987).
45. LEPTO 6.5, G. Ingelman, A. Edin, J. Rathsman, Comp. Phys. Commun. 101 (1997) 108.
46. HERWIG 5.1, G. Marchesini et al., Comp. Phys. Commun. 67 (1992) 465.
47. L. Lönnblad, Proc. of the workshop "Monte Carlo Generators for HERA Physics", 1998-1999, DESY, Hamburg (to be published).
48. I.M. Dremin and V.A. Nechitailo, Mod. Phys. Lett. A9 (1994) 1471; I.M. Dremin and R.C. Hwa, Phys. Lett. B324 (1994) 477; Phys. Rev D49 (1994) 5805.
49. H1 Collaboration, C. Adloff et al., Eur. Phys. J. C5 (1998) 625; ZEUS Collaboration, paper No. 806 submitted to ICHEP98 Vancouver Conference, July 1998.